SEDIMENT TRANSPORT SIMULATION APPLICABLE TO A WIDE CONCENTRATION RANGE

Nicolas Eko Saputra[1], Takaaki Shigematsu[2] and Gozo Tsujimoto[3]

Recent video images of tsunami attacks clearly show that tsunamis transport sediment from the seabed and riverbeds to land. Some studies also pointed out that sediment-containing fluids have a greater density than fresh water, so the hydrodynamic force acting on structures is more significant than that of pure water. However, it is common practice to use the advection-diffusion equation to estimate sediment transport by the tsunami, and the effect of the sediment concentration in the water on tsunami propagation needs to be taken into account. In this study, we solved the motion equation, which can take into account the effects of sediment in the water on tsunami propagation and run-up. We used a sediment transport model that does not rely on the advection-diffusion equation to predict tsunami damage associated with the Nankai Trough earthquake. The present model shows that the propagation velocity of a tsunami with a high concentration is faster than that of a low concentration.

Keywords: sediment transport; mixture model; tsunami

MAIN SECTION

STUDY BACKGROUND AND TARGET

Massive trench-type earthquakes can sometimes trigger huge tsunamis, a fact that commands our respect for the power of nature. The 2011 Tohoku earthquake and tsunami, a prime example of this, was a staggering event. On 11 March 2011, a substantial undersea earthquake of magnitude 9.0 occurred off the east coast of the Oshika Peninsula, the strongest ever recorded in Japan. This earthquake set off a tsunami of monumental proportions, with a maximum wave height of 40.5 m (Cabinet Office, 2011), causing extensive damages in Japan's Tohoku region.

In addition to the damage caused by the tsunami, it also carried large amounts of sediment inland and deposited it. In Miyagi Prefecture, sediment deposits of an average of 5 to 10 cm and a maximum of 40 cm were recorded in coastal areas (Komai et al. 2012). This sedimentation significantly hindered rescue, relief, and evacuation activities in coastal and nearby urban areas. Because the sediment transported by the tsunami contains various substances derived from seawater, it could harm public health if the sediment accumulates over a long period. In order to address these issues, it is important to predict the amount of sediment transported to land by the tsunami as accurately as possible and to take prompt measures.

Many sediment transport forecasting techniques were established long before the 2011 Tohoku earthquake and tsunami. One of the most commonly utilized methodology is the approach proposed by Takahashi et al. (1999). This model considers sediment exchange between the bedload layer, which encompasses the upwelling of sediment from the seabed and its subsequent deposition on the seabed, and the suspended sediment layer, where sediment is transported over a vast area by water currents. In the bedload layer, the quantity of sediment upwelled is defined by the magnitude of the shear stress acting on the seabed. In the suspended sediment layer, the sediment transport is calculated by solving the advection-diffusion equation. This method has been utilized in numerous studies (e.g., Kondo et al., 2011; Sugawara et al., 2014), and its efficacy in predicting sediment behavior during tsunamis has been demonstrated.

However, most of the existing sediment transport models, including the aforementioned research, are based on the assumption of low sediment concentration in water. As a result, these models do not consider the effect of sediment in the water on tsunami propagation. In other words, these models are unidirectional, with the tsunami current acting as the driving force behind sediment transport. They do not, however, account for the effect of sediment in water on the movement of water. However, this research focuses on developing a sediment transport model that can be applied even when the sediment concentration is high. When the sediment concentration is high, the hydrodynamic forces acting between the sediment and water become significant, and it is important to consider these interactions. The interaction between sediment and water plays a much more significant role under these conditions (Gotoh 2004).

To calculate the interaction force between water and sediment, we apply a mixture model that treats the sediment contained in the water as a dispersed phase and solves for the time-space variation of the

[1] Osaka Metropolitan University, su23213g@st.omu.ac.jp.
[2] Osaka Metropolitan University, shige@omu.ac.jp.
[3] Toyo Construction Co., LTD., Tsujimoto-gozo@toyo-const.co.jp

volume ratio of both this dispersed phase and the continuous phase of water (Ishii 1975). The mixture model is an efficient solution for handling the significant computational demands of tsunami simulations over a wide range while accounting for local dispersed phase-continuous phase interactions. This study aims to develop a method for accurately predicting the behavior of turbid water masses with a wide range of sediment concentrations during a tsunami using this mixed model. We will use the developed method to simulate sediment transport during a Nankai Trough earthquake tsunami and predict the resulting sediment deposition. Finally, we will compare the sediment deposition thickness predicted by the mixed model with the results of the conventional model.

NUMERICAL METHOD

THE DERIVATION OF MIXTURE MODEL

This study will calculate sediment transport due to the tsunami using the mixture model (Ishii 1975, Mikko et al. 1996, Ishii et al. 2006). The mixture model treats the water containing sediment as a two-phase flow of the continuum (water) and dispersed (sediment) phases. The main feature of the mixture model is that the equations of motion for both phases can be combined and solved using a single equation. First, it will start by defining the basic formula for applying the mixture model to the analysis of tsunami propagation, including sediment.

First, consider a control volume that contains specific amounts of suspended sediment within water. The volumes of both the continuum and dispersed phases in this control volume are represented respectively as volume fractions α_1 and α_2 (see Fig. 1). Herein,

$$\alpha_1 + \alpha_2 = 1 \tag{1}$$

must be satisfied. The subscripts 1 and 2 represent continues and dispersed phases, respectively.

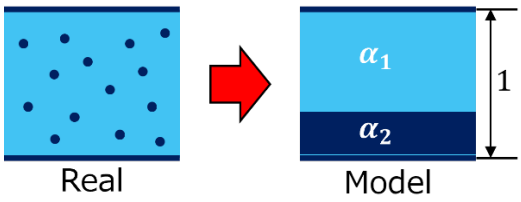

Figure 1. Volume fractions of the continuum phase and dispersed phase in a control volume

In the phenomenon that this research targets, the density of the water containing sediment increases as the sediment on the seabed is swept up into the water by the flow caused by the tsunami. This multiphase fluid's density (ρ_m) and velocity (u_m) are calculated as functions of the volume fraction using the following equations.

$$\rho_m = \rho_1\alpha_1 + \rho_2\alpha_2 \tag{2}$$

$$\boldsymbol{u}_m = \frac{1}{\rho_m}(\boldsymbol{u}_1\rho_1\alpha_1 + \boldsymbol{u}_2\rho_2\alpha_2) \tag{3}$$

where $\boldsymbol{u}$ and ρ represent the velocity vector and density, respectively.

The continuity equations for each phase can be expressed as follows:

$$\frac{\partial}{\partial t}(\alpha_1\rho_1) + \nabla\cdot(\alpha_1\rho_1\boldsymbol{u_1}) = \Gamma_1 \tag{4}$$

$$\frac{\partial}{\partial t}(\alpha_2\rho_2) + \nabla\cdot(\alpha_2\rho_2\boldsymbol{u_2}) = \Gamma_2 \tag{5}$$

here Γ_1 and Γ_2 represent the generation rates for each phase, and their sum must equal zero ($\Gamma_1 + \Gamma_2 = 0$) to maintain mass conservation. By taking the sum of equations (4) and (5) and using the relational equations of equations (2) and (3), the following continuous equation as a mixed model is obtained:

$$\frac{\partial \rho_m}{\partial t} + \nabla \cdot (\rho_m \boldsymbol{u_m}) = 0 \tag{6}$$

A similar approach is applied to the momentum equations. The momentum equations for each phase are expressed as:

$$\frac{\partial}{\partial t}(\alpha_1 \rho_1 \boldsymbol{u_1}) + \nabla \cdot (\alpha_1 \rho_1 \boldsymbol{u_1 u_1}) = -\alpha_1 \nabla p_1 + \nabla \cdot \alpha_1 (\boldsymbol{\tau}_1 + \boldsymbol{\tau}_{T1}) + \alpha_1 \rho_1 \boldsymbol{g} + \boldsymbol{M}_1 \tag{7}$$

$$\frac{\partial}{\partial t}(\alpha_2 \rho_2 \boldsymbol{u_2}) + \nabla \cdot (\alpha_2 \rho_2 \boldsymbol{u_2 u_2}) = -\alpha_2 \nabla p_2 + \nabla \cdot \alpha_2 (\boldsymbol{\tau}_2 + \boldsymbol{\tau}_{T2}) + \alpha_2 \rho_2 \boldsymbol{g} + \boldsymbol{M}_2 \tag{8}$$

where p is the pressure, $\boldsymbol{\tau}$ and $\boldsymbol{\tau}_{T1}$ represent viscosity and turbulent stress terms, $\boldsymbol{g}$ is the gravitational force, and $\boldsymbol{M}$ is the interfacial interaction term between continuum and dispersed phases. $\boldsymbol{M}_1$ and $\boldsymbol{M}_2$ have an action-reaction relationship, so $\boldsymbol{M}_1 + \boldsymbol{M}_2 = 0$. The sum of the second terms on the left-hand side of the momentum equations of each phase can be expressed as:

$$\nabla \cdot (\alpha_1 \rho_1 \boldsymbol{u}_1 \boldsymbol{u}_1) + \nabla \cdot (\alpha_2 \rho_2 \boldsymbol{u}_2 \boldsymbol{u}_2) = \nabla \cdot (\rho_m \boldsymbol{u}_m \boldsymbol{u}_m) + \nabla \cdot \sum_{k=1}^{2} \alpha_k \rho_k \boldsymbol{u}_{km} \boldsymbol{u}_{km} \tag{9}$$

where $\boldsymbol{u}_{km}$ is the velocity of each phase $k(=1,2)$ relative to the mass mixture center, defined as $\boldsymbol{u}_{km} = \boldsymbol{u}_k - \boldsymbol{u}_m$. Using equation(9), we can sum equations (7) and (8) to derive the following equation.

$$\frac{\partial}{\partial t}(\rho_m \boldsymbol{u_m}) + \nabla \cdot (\rho_m \boldsymbol{u_m u_m}) + \nabla \cdot \sum_{k=1}^{2} \alpha_k \rho_k \boldsymbol{u}_{km} \boldsymbol{u}_{km} = -\nabla p_m + \nabla \cdot (\boldsymbol{\tau_m} + \boldsymbol{\tau_{Tm}}) + \rho_m \boldsymbol{g} \tag{10}$$

As discussed below, the interfacial interaction force is formulated as the relative velocity of each phase to the multiphase fluid, as shown in the following equation.

$$\boldsymbol{u}_{1m} = \boldsymbol{u}_1 - \boldsymbol{u}_m \tag{11}$$

$$\boldsymbol{u}_{2m} = \boldsymbol{u}_2 - \boldsymbol{u}_m \tag{12}$$

Using equations (2) and (3), equations (11) and (12) can be rewritten as follows.

$$\boldsymbol{u}_{1m} = \left(1 - \frac{\alpha_1 \rho_1}{\rho_m}\right) \boldsymbol{u}_{12} \tag{13}$$

$$\boldsymbol{u}_{2m} = \left(1 - \frac{\alpha_2 \rho_2}{\rho_m}\right) \boldsymbol{u}_{21} \tag{14}$$

where, $\boldsymbol{u}_{21} = \boldsymbol{u}_2 - \boldsymbol{u}_1$ represents the dispersed phase velocity relative to the continuum phase. To derive the relative velocity ($\boldsymbol{u}_{21}$), the assumption that the pressure is the same in both phases is introduced ($p_m = p_1 = p_2$). Using the relationships in equations (8) and (10), the following equation is obtained.

$$\begin{aligned}\boldsymbol{M}_2 = \alpha_2 \left[\rho_2 \frac{\partial \boldsymbol{u}_{2m}}{\partial t} + (\rho_2 - \rho_m)\frac{\partial \boldsymbol{u}_m}{\partial t}\right] \\ + \alpha_2[\rho_2(\boldsymbol{u}_2 \cdot \nabla)\boldsymbol{u}_2 - \rho_m(\boldsymbol{u}_m \cdot \nabla)\boldsymbol{u}_m] \\ + \nabla \cdot [\alpha_2(\boldsymbol{\tau}_2 + \boldsymbol{\tau}_{T2})] \\ + \alpha_2 \nabla \cdot \left[\left(\boldsymbol{\tau}_m + \boldsymbol{\tau}_{Tm} + \left(\sum_{k=1}^{2} \alpha_k \rho_k \boldsymbol{u}_{km}\boldsymbol{u}_{km}\right)\right)\right] \\ - \alpha_2(\rho_2 - \rho_m)\boldsymbol{g}\end{aligned} \tag{15}$$

To simplify the derivation of the interfacial interaction force ($\boldsymbol{M}_2$), some assumptions are introduced. First, the time derivative of the dispersed phase velocity relative to the multiphase flow ($\partial \boldsymbol{u}_{2m}/\partial t$) is assumed to be small enough and negligible. Furthermore, the term $(\boldsymbol{u}_2 \cdot \nabla)\boldsymbol{u}_2$ is assumed to be equal to $(\boldsymbol{u}_m \cdot \nabla)\boldsymbol{u}_m$. Moreover, $\boldsymbol{\tau}_m + \boldsymbol{\tau}_{Tm} + (\sum_{k=1}^{2} \alpha_k \rho_k \boldsymbol{u}_{km}\boldsymbol{u}_{km})$ is assumed to be very small compared to other terms and neglected. Applying these assumptions, equation (15) can be simplified as follows:

$$\boldsymbol{M_2} = \alpha_2(\rho_2 - \rho_m)\left[\frac{\partial u_m}{\partial t} + (\boldsymbol{u}_m \cdot \nabla)\boldsymbol{u}_m - \boldsymbol{g}\right] \tag{16}$$

On the other hand, following Ishii et al. (2006), the interfacial interaction force $\boldsymbol{M}_2$ is formulated as a linear combination of various known interaction forces.

$$\boldsymbol{M_2} = \frac{\alpha_2}{V_2}\left(\boldsymbol{F_2}^{\boldsymbol{D}} + \boldsymbol{F_2}^{\boldsymbol{V}} + \boldsymbol{F_2}^{\boldsymbol{B}} + \boldsymbol{F_2}^{\boldsymbol{L}} + \boldsymbol{F_2}^{\boldsymbol{W}} + \boldsymbol{F_2}^{\boldsymbol{T}}\right) \tag{17}$$

where V_2 represents the volume of a sediment particle, $\boldsymbol{F_2}^{\boldsymbol{D}}$is the drag force, $\boldsymbol{F_2}^{\boldsymbol{V}}$is the virtual mass force, $\boldsymbol{F_2}^{\boldsymbol{B}}$is the Basset force, $\boldsymbol{F_2}^{\boldsymbol{L}}$is the lift force normal, $\boldsymbol{F_2}^{\boldsymbol{W}}$ is the wall lift force, and $\boldsymbol{F_2}^{\boldsymbol{T}}$is the turbulent dispersion force. In this study, all forces beside the drag force are neglected. Equation (17) then can be rewritten as follows.

$$\boldsymbol{M_2} = \frac{\alpha_2}{V_2}\left(-\frac{1}{2}C_D\rho_2\boldsymbol{u}_{21}|\boldsymbol{u}_{21}|A_2\right) \tag{18}$$

where A_2 represents the particle's projected area, and C_D is the drag force coefficient. In this study, the drag force coefficient proposed by Schiller & Nauman (Clift et al. 1978) will be used, defined as follows.

$$\begin{aligned} C_D &= \frac{24}{Re}(1 + 0.15Re^{0.687}) && Re < 1000 \\ C_D &= 0.44 && Re \geq 1000 \end{aligned} \tag{19}$$

where Re is the Reynolds number which is defined as follows:

$$Re = \frac{d\rho_2|\boldsymbol{u}_{21}|}{\mu_m} \tag{20}$$

where μ_m represents the viscosity coefficient of the mixture fluid, d represents the particle's diameter. By substituting the drag coefficient (C_D) to $\frac{24}{Re}C_D$, the relationship in equation (18) can be rewritten as follows:

$$\boldsymbol{M}_2 = -\frac{18\alpha_2\mu_m C_D}{d^2}\boldsymbol{u}_{21} \tag{21}$$

thus, equation (19) will be rewritten as follows:

$$\begin{aligned} C_D &= (1 + 0.15Re^{0.687}) && Re < 1000 \\ C_D &= 0.0183Re && Re \geq 1000 \end{aligned} \tag{22}$$

Finally, by substituting equation (21) into equation (16), the relative velocity of the dispersed phase with respect to the continuum phase ($\boldsymbol{u}_{21}$) can be derived as:

$$\boldsymbol{u}_{21} = \frac{{d_2}^2(\rho_2 - \rho_m)}{18\mu_m C_D}\left[\boldsymbol{g} - (\boldsymbol{u}_m \cdot \nabla)\boldsymbol{u}_m - \frac{\partial \boldsymbol{u}_m}{\partial t}\right] \tag{23}$$

APPLIANCE OF MIXTURE MODEL TO TSUNAMI GOVERNING EQUATIONS

Figure 2 shows the coordinate settings used in this study to calculate the water depth and the surface water elevation.

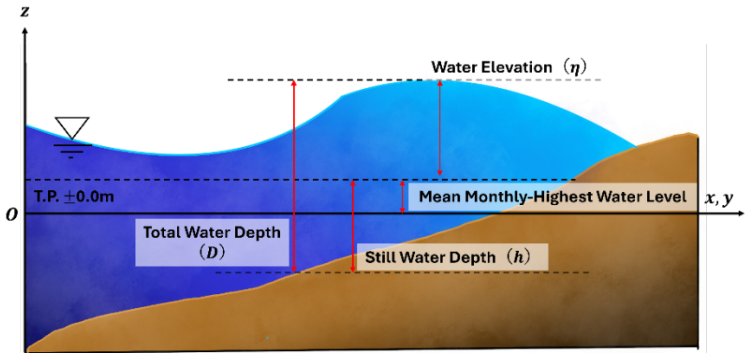

Figure 2. Schematic illustration of water depth and coordinate

The tsunami propagation was calculated by solving the equations obtained by integrating the equations of the mass conservation and the motion of the mixture fluid containing sediments, considering the density in the vertical direction.

$$\rho_m \frac{\partial D}{\partial t} + \frac{\partial}{\partial x}(\rho_m M_m) + \frac{\partial}{\partial y}(\rho_m N_m) = 0 \tag{24}$$

$$\begin{aligned} &\rho_m \frac{\partial M_m}{\partial t} + \frac{\partial}{\partial x}\left(\frac{\rho_m {M_m}^2}{D}\right) + \frac{\partial}{\partial y}\left(\frac{\rho_m M_m N_m}{D}\right) + \frac{\partial}{\partial y}\left(\frac{\alpha_2 \rho_2 M_{2m} N_{2m}}{D}\right) \\ &\quad + \frac{\partial}{\partial x}\left(\frac{\alpha_1 \rho_1 {M_{1m}}^2}{D}\right) + \frac{\partial}{\partial x}\left(\frac{\alpha_2 \rho_2 {M_{2m}}^2}{D}\right) \\ &\quad + \frac{\partial}{\partial y}\left(\frac{\alpha_1 \rho_1 M_{1m} N_{1m}}{D}\right) \\ &\quad = -\rho_m g D \frac{\partial \eta}{\partial x} - \frac{\rho_m g n^2}{D^{7/3}} M_m \sqrt{{M_m}^2 + {N_m}^2} \end{aligned} \tag{25}$$

$$\begin{aligned} &\rho_m \frac{\partial N_m}{\partial t} + \frac{\partial}{\partial x}\left(\frac{\rho_m M_m N_m}{D}\right) + \frac{\partial}{\partial y}\left(\frac{\rho_m {N_m}^2}{D}\right) + \frac{\partial}{\partial x}\left(\frac{\alpha_2 \rho_2 M_{2m} N_{2m}}{D}\right) \\ &\quad + \frac{\partial}{\partial y}\left(\frac{\alpha_2 \rho_2 {N_{2m}}^2}{D}\right) + \frac{\partial}{\partial x}\left(\frac{\alpha_1 \rho_1 M_{1m} N_{1m}}{D}\right) \\ &\quad + \frac{\partial}{\partial y}\left(\frac{\alpha_1 \rho_1 {N_{1m}}^2}{D}\right) \\ &\quad = -\rho_m g D \frac{\partial \eta}{\partial y} - \frac{\rho_m g n^2}{D^{7/3}} N_m \sqrt{{M_m}^2 + {N_m}^2} \end{aligned} \tag{26}$$

where M_m and N_m represent the depth-integrated flow fluxes of mixture fluid in the x and y direction, respectively. Similarly, M_{1m}, N_{1m}, M_{2m}, N_{2m} represent the depth-integrated relative flow fluxes in the x- and y- axes for the liquid and solid phases. The subscripts 1 and 2 refer to liquid phase and solid phase respectively. D represents the total water depth, calculated as the sum of the water surface elevation (η) and the still water depth (h), n is the manning roughness coefficient. Using the derived equation for relative velocity, and the relationships in equations (13) and (14), the relative follow fluxes can be calculated as follows.

$$M_{1m} = \left(\frac{\alpha_1\rho_1}{\rho_m} + 1\right) M_{21}, \quad N_{1m} = \left(\frac{\alpha_1\rho_1}{\rho_m} + 1\right) N_{21} \tag{27}$$

$$M_{2m} = \left(1 - \frac{\alpha_2\rho_2}{\rho_m}\right) M_{21}, \quad N_{2m} = \left(1 - \frac{\alpha_2\rho_2}{\rho_m}\right) N_{21} \tag{28}$$

$$M_{21} = \frac{d^2(\rho_2 - \rho_m)}{18\mu_m C_D}\left(-\frac{\partial}{\partial x}\left(\frac{{M_m}^2}{D}\right) - \frac{\partial M_m}{\partial t}\right) \tag{29}$$

$$N_{21} = \frac{d^2(\rho_2 - \rho_m)}{18\mu_m C_D}\left(-\frac{\partial}{\partial y}\left(\frac{{N_m}^2}{D}\right) - \frac{\partial N_m}{\partial t}\right) \tag{30}$$

Additionally, in this study the viscosity coefficient for the mixture liquid will be calculated using the following equation:

$$\mu_m = \mu_1\left(1 - \frac{\alpha_2}{0.62}\right)^{-1.55} \tag{31}$$

where μ_1 represents the viscosity coefficient of pure water at 20℃.

THE GOVERNING EQUATIONS OF SEDIMENT TRANSPORT

Sediment transport is calculated by sediment transport in the bedload layer, which is directly related to the sea bed deformation, and sediment transport in the suspended sediment layer, which is transported by flow (Takahashi et al. 1999) as shown in the schematic illustration, Figure 3.

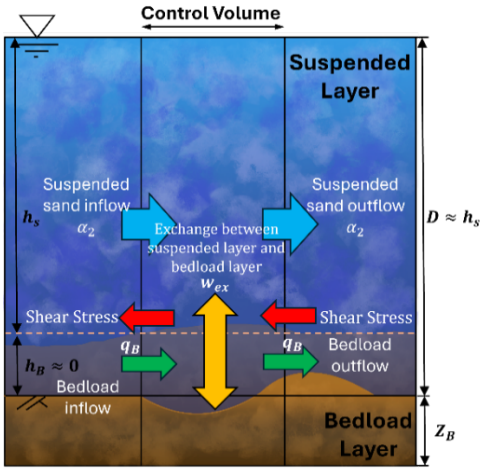

Figure 3. Diagram about sediment transport calculation in this study

Seabed erosion occurs as significant bottom shear stress acts on the seabed. The bedload transport rate q_B is calculated using the following equation.

$$q_B = \alpha\sqrt{sgd^3}(\tau_* - \tau_{cr})^{3/2} \tag{32}$$

where $\alpha = 5.95$ is the bedload sediment coefficient, s is the submerged density of the sediment particle, $\tau_* = {u_*}^2/sgd$ is the Shield parameter, and $\tau_{cr} = {u_{cr}}^2/sgd$ is the critical value of the Shields parameter for initiating sediment movement. To incorporate the effect of seabed slope in the bedload transport, equation (32) is rewritten as (Sugawara et al. 2014).

$$Q_B = q_B - |q_B|\varepsilon\frac{\partial Z_B}{\partial x} - |q_B|\varepsilon\frac{\partial Z_B}{\partial y} \tag{33}$$

where Z_B represents the seabed elevation, $\varepsilon = 2.5$ represents the parameter related to the diffusion coefficient of the sediments. The change in seabed elevation due to bedload transport can then be calculated using the following equation.

$$\frac{\partial Z_B}{\partial t} + \frac{1}{1-\lambda}\left(\frac{\partial Q_{bx}}{\partial x} + \frac{\partial Q_{by}}{\partial y} + w_{ex}\right) = 0 \tag{34}$$

where $\lambda = 0.4$ represents the void ratio of the seabed. The exchange rate w_{ex} is calculated using the following equation considering the balance of sediment picked up from the seabed and sediment settlement from the suspended layer into the bedload layer.

$$w_{ex} = \beta\sqrt{sgd}(\tau_* - \tau_{cr})^2 - w_o\alpha_2 \tag{35}$$

where $\beta = 9.0 \times 10^{-5}$ represents the suspended sediment coefficient. The particle's settlement velocity w_o is calculated using the Rubey Equation (Rubey 1933).

$$w_o = \sqrt{sgd}\left(\sqrt{\frac{3}{2} + \frac{36{\nu_m}^2}{sgd^3}} - \sqrt{\frac{36{\nu_m}^2}{sgd^3}}\right) \tag{36}$$

where ν_m represents the dynamic viscosity coefficient for the mixture fluid, which can be obtained as $\nu_m = \mu_m/\rho_m$. The suspended sediment transport can be calculated by solving the following equation obtained by integrating the sediment transport equation along the depth direction containing the exchange rate w_{ex}.

$$\frac{\partial \alpha_2 D}{\partial t} + \frac{\partial \alpha_2 M_m}{\partial x} + \frac{\partial \alpha_2 N_m}{\partial y} - w_{ex} = -\frac{\partial \alpha_2 M_{2m}}{\partial x} - \frac{\partial \alpha_2 N_{2m}}{\partial y} \tag{37}$$

Morishita et al. (2014) introduced a calculation method of saturated suspended sediment concentration to avoid excessive sediment concentration in the suspended layer. While there is limited scientific knowledge about the precise value of this concentration, a value of 0.01 (1%) is often used based on empirical experience (e.g. Kondou et al. 2011 and Murakami et al. 2018). Some studies have also adjusted the saturated suspended sediment concentration based on flow conditions (e.g. Arimitsu et al. 2017 and Yamashita et al. 2018). However, introducing the saturated suspended sediment concentration can lead to underestimating sediment accumulation on land. Therefore, in this study, we will not implement a saturated suspended sediment concentration.

NUMERICAL EXPERIMENT

To distinguish the differences between the conventional model and the mixture model, a numerical experiment using a dam-break wave was conducted. In the experiment, the water column with an initial water elevation η of 0.06 m in the reservoir was released. The calculated results between with $\alpha_2 = 0.1$ and without sediment concentrations $\alpha_2 = 0.0$ are compared.

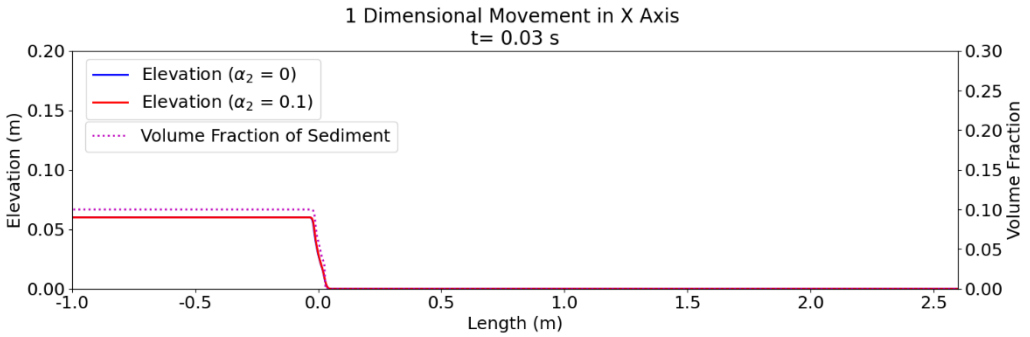

(a) t = 0.03s

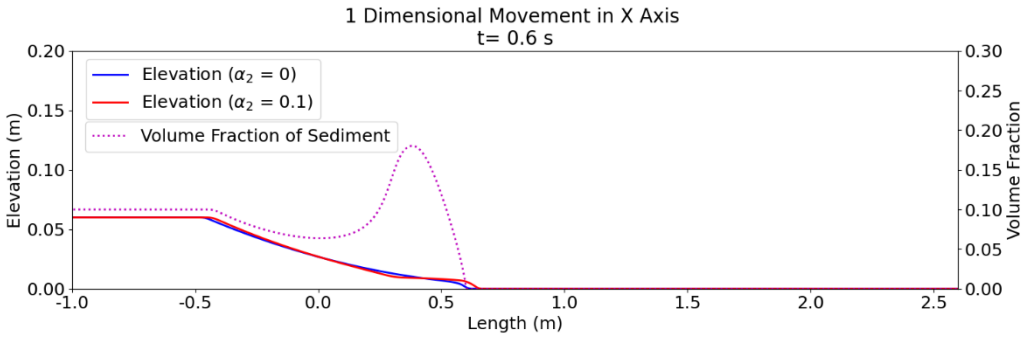

(b) t = 0.6s

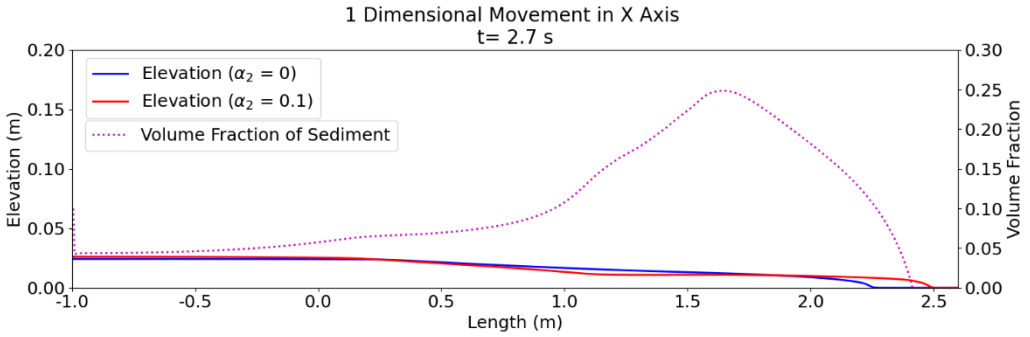

(c) t = 2.7s

Figure 4. Calculated results of dam-break wave propagation

Figure 4 presents the result of the numerical experiment on dam-break wave propagations. It is found from Figure 4 that the tip velocity of the dam-break wave with sediment is faster than that without sediment. This is thought to be due to the fact that the density of water containing suspended sand is greater than that of water without suspended sand, resulting in greater momentum.

CALCULATION CONDITIONS FOR TSUNAMI PROPAGATION

This study examines the effects of the Nankai Trough Earthquake Tsunami on the coastal land area in Osaka City. To investigate the sediment accumulation in the land area, the calculation results from the conventional model and the mixture model will be compared.

Table 1 presents the calculation conditions used. The calculation area is divided into five regions with varying grid sizes. Nesting calculations are performed between these regions to determine the boundary conditions for subsequent areas.

Table 1. Calculation Parameters

No	Parameter	Calculation Condition
1	Fault model	Nankai Trough Earthquake Investigation Committee Case 5
2	Grid size	810 m, 270 m, 90 m, 30 m, 10 m
3	Calculation time	6 hours
4	Tide Height on typhoon season	T.P. +0.9 m
5	Sand diameter	0.05 mm
6	Bedload sediment coefficient α	5.95
7	Suspended sediment coefficient β	9.0×10^{-5}
8	Critical Friction Velocity	1.06×10^{-2}m/s

The calculation areas are shown in figure 5.

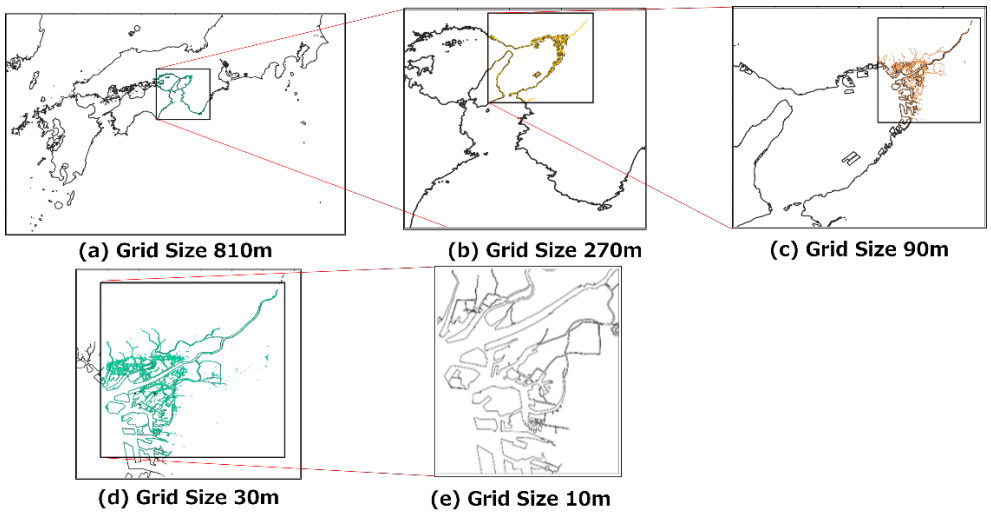

Figure 5. Target areas for calculation

CALCULATION RESULTS AND DISCUSSION

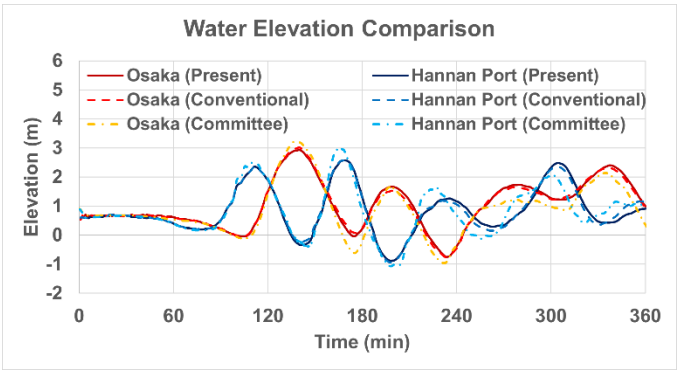

(a) Water surface elevation

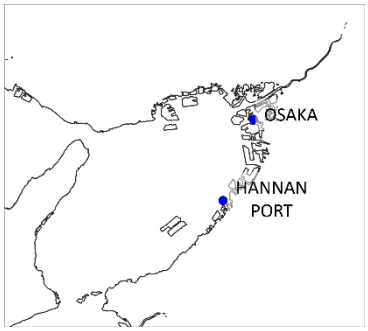

(b) Water level extraction point

Figure 6. Comparison of water elevation between the conventional model and the mixture model

Figure 6(a) presents the calculated results of water surface elevation results by the conventional model and the mixture model developed by this study, alongside the results from the Nankai Trough Earthquake Investigation Committee (referred to as "the committee" hereafter). Figure 6(b) indicates the extraction point for the water elevation data shown in Figure 6(a). Both models produce reasonable results, and when compared to the committee's calculation, they demonstrate satisfactory accuracy.

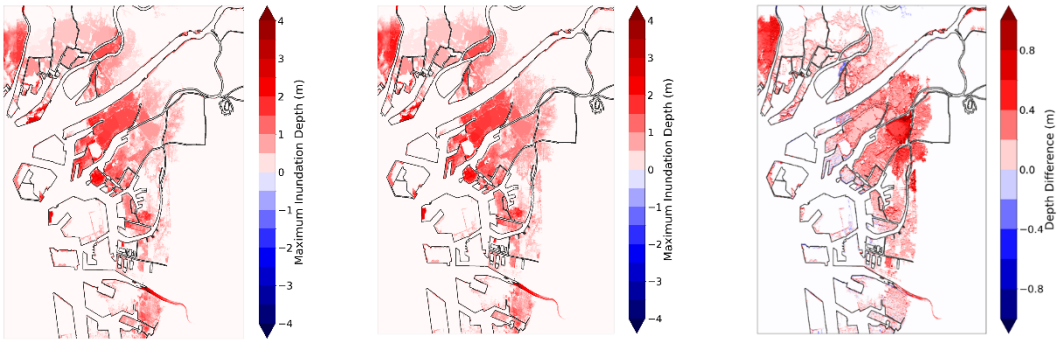

(a) Conventional model (b) Mixture model (c) The differences between both model

Figure 7. Maximum water depth during tsunami inundation

Figures 7(a) and 7(b) show the distribution of the maximum flood depth during the tsunami inundation simulated using the conventional model and the mixture model, respectively. Figure 7(c) presents the difference between the results of the mixture model (Figure 7(b)) and the conventional model (Figure 7(a)). From Figure 7(c), it is evident that the maximum flood depth estimated by the mixture model is greater than that of the conventional model. This difference is particularly noticeable in the northeastern part of the city, where the maximum inundation depth is 0.4 to 0.6 m higher.

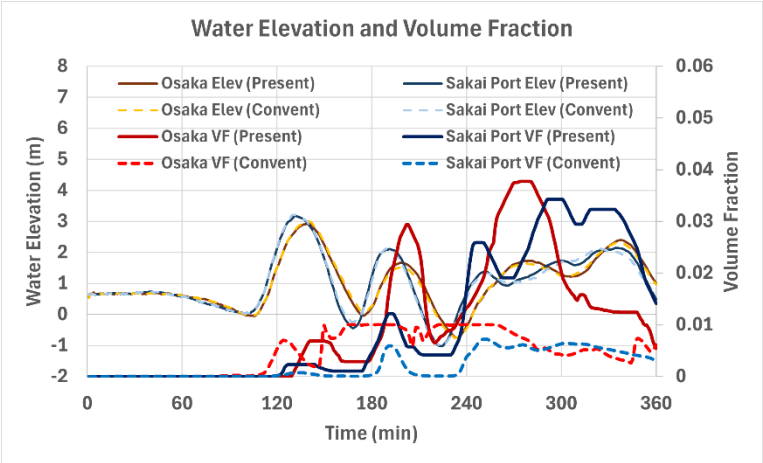

Figure 8. Comparison of volume fraction of sediment

Figure 8 illustrates the time series of sediment volume fraction (i.e. sediment concentration) and tsunami elevation simulated using both models at Osaka and Sakai Port (refer to Figure 9 for extraction location). In the figure's legend, "Elev" represents water elevation, "FV" represents volume fraction. "Present" refers to the calculation results of the model used in the present study, and "Convent" refers to the calculation results of the conventional model. According to the figure, the sediment concentration calculated using the conventional model does not exceed 0.01 because of the limitation of the saturated sediment concentration. In contrast, the mixture model yields significantly higher sediment concentrations. Another notable characteristic observed in the graph is the process by which sediment concentration builds up. Figure 9 shows the distribution of suspended sediment concentration 150 minutes after the earthquake occurred. From these figures, there is a significant difference in the spatial distribution of suspended sediment concentration between the conventional model with a saturation limit for suspended sediment concentration and the model developed in this study.

Figure 10 presents the distribution of sediment accumulation on land. Since most of the land surface in the Osaka metropolitan area is covered with asphalt, the calculation of sediment transport on land in this study does not consider erosion but only the deposition of suspended sediment. Comparing the two results in Figure 10, the conventional model shows that nearly all areas in Osaka City are covered by sediment with a thickness of approximately 0.01 m, with a small portion reaching up to 0.1 meters, particularly in riverbed areas. The area of sand deposition on land calculated using the mixed model is

almost the same as that calculated using the conventional model, but the thickness of the deposits is significantly greater. In particular, the maximum thickness of the sediment reaches 0.4 m in the northern part of the city, where the zero-metre zone extends. It was reconfirmed that the saturated suspended sediment concentration has a significant impact on the accurate estimation of sediment accumulation in land areas.

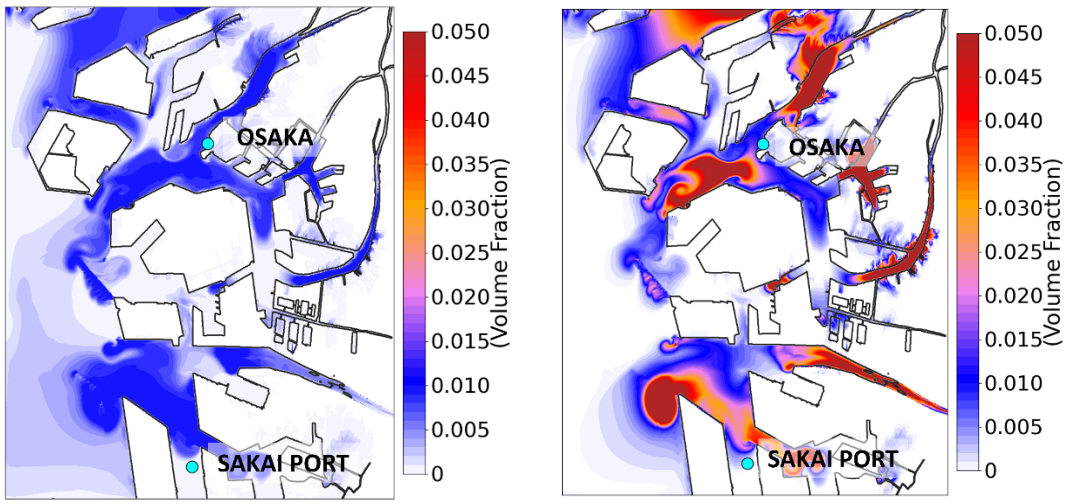

(a) Conventional model **(b) Mixture model**

Figure 9. Suspended sediment concentration (t = 150 min.)

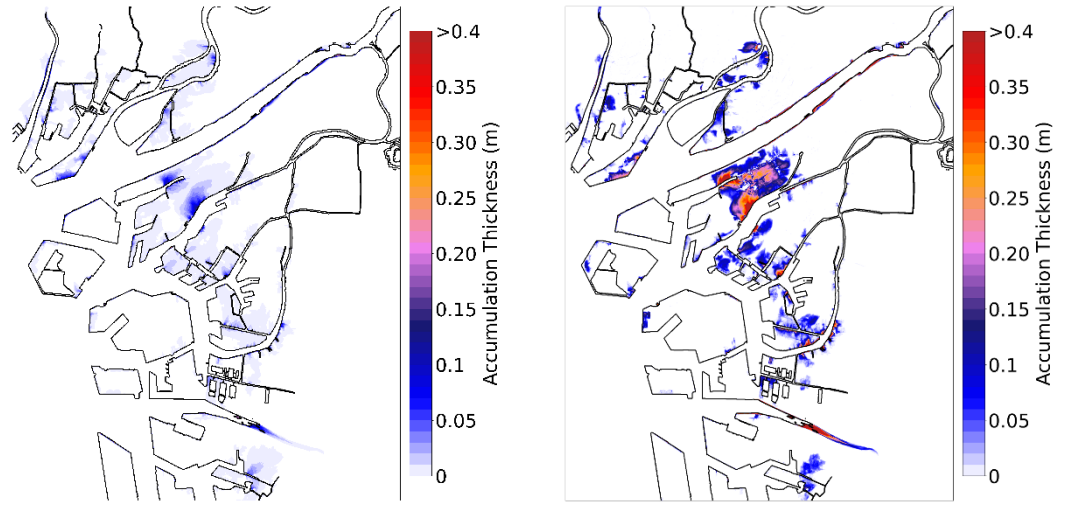

(a) Conventional model **(b) Mixture model**

Figure 10. Distribution of sediment accumulation on the land of Osaka City

CONCLUSION

In this study, tsunami propagation and sediment distribution caused by the Nankai Trough Earthquake Tsunami were calculated using both the conventional model and the mixture model. Based on the discussion above, the conclusions of this study are summarized as follows:

1. The higher the sediment concentration in the water column, the faster the wave propagates. This occurs because the inclusion of more sediment increases the fluid's density, resulting in greater momentum and energy, which allows the wave to travel faster than pure water.
2. There is a small difference in the tsunami arrival time between the conventional model and the mixture model. This is because, in coastal areas, the sediment concentration in the water is relatively low compared to that on land, leading to only a slight increase in propagation velocity.

3. The propagation velocity on land is higher in the mixture model, resulting in a greater maximum flood depth, particularly in urban areas. The norther part of the city, where the tsunami halted, experienced the highest flood depths.
4. The sediment concentration trends differ significantly between the conventional model and the mixture model. In the conventional model, the sediment concentration is capped at 0.01 (1%) due to the imposed saturation limit. In contrast, the mixture model shows a rapid increase in sediment concentration, particularly 180 minutes after the simulation began, coinciding with the arrival of the tsunami's second wave.
5. The mixture model predicts significantly higher sediment accumulation on land compared to the conventional model. This increased sediment accumulation could severely hinder rescue, relief, and evacuation efforts in the affected areas.

ACKNOWLEDGMENTS

The authors gratefully acknowledge the support provided by OMU Spring Scholarship under grand number RS23A016 for funding this research.

REFERENCES

Arimitsu T., Matsuda S., Murakami Y., Shikata T., Kawasaki K., Mishima T., Shimizu R., Sugawara D. 2017. Influence of Computational Parameters on Accuracy of Moveable Bed Model for Tsunamis. Journal of JSCE. 73(2), I_589-I_594.

Cabinet Office. 2011. Great East Japan Earthquake, Special Edition. https://bousai.go.jp/kohou/kouhoubousai/h23/63/special_01.html. Accessed 25 November 2024.

Clift, R., Grace, J. R., Weber, M. E. 1978. Bubbles, Drops, and Particles. Academic Press, 111 p. London.

Gotoh H. 2004. Computational Mechanics of Sediment Transport. Morikita Publishing Co., Ltd, 223 pp.

Ishii M. 1975. Thermo-dynamic theory of two-phase flow. NasaSTI/Recon Technical Report A.

Ishii M., Hibiki T. 2006. Thermo-Fluid Dynamics of Two-Phase Flow. Springer, New York.

Komai T., Kawabe Y., Hara J., Sakamoto Y., Zhang M. 2012. Urgent Investigation of tsunami deposits at coastal areas of eastern Japan -environmental risk caused by tsunami deposits-. *GSJ Geology News,* Vol. 1 No. 6, 181-184.

Kondou T., Morimoto T., Fujimoto N., Tonomo K., Iemura K., Shikata T. 2011. Influence of the Port Facilities by the Sediment Transport due to Tsunami. *Journal of JSCE*. 67(2), I_261-I_265.

Manninen M., Taivassalo V. 1996. On the mixture model for multiphase flow. VTT Publications 288.

Morishita Y., Takahashi T. 2014. Accuracy improvement of movable bed model for tsunamis by applying for Kesennuma bay when the 2011 Tohoku tsunami arrived. *Journal of JSCE*. 70(2), I_491-I_495.

Murakami Y., Shikata T., Tonomo K., Sugawara D., Hiraishi T. 2018. Study on Setting of Saturation Concentration of Suspended Sediment in Numerical Simulation of Sediment Transport Associated with Tsunami for off Takahama Bay. Journal of JSNDS. 37(2), 165-176.

Rubey W.W. 1933. Settling Velocity of Gravels, Sand, and Silt Particles. Am. J. Sci. Vol. 25, pp. 325-338

Sugawara D., Takahashi T., Imamura F. 2014. Sediment Transport due to the 2011 Tohoku-oku Tsunami at Sendai: Result from Numerical Modeling. *International Journal of Marine Geology*. 358, 18-37.

Takahashi T., Shutou N., Imamura F., Asai Daisuke. 1999. Development of a Tsunami Moving Bed Model with the Amount of Exchanged Bed Load Layer and Suspended Sediment Layer Considered. *Journal of JSCE*, 46, 606-610.

Yamashita K., Sugawara D., Arakawa T., Shigihara Y., Takahashi T., Imamura F. 2018. Improvement of Tsunami-Induced Sediment Transport Model by Considering Saturated Concentration in Suspension with Strong Unsteady Flows. Journal of JSCE. 74(2), I_325-I_330.